J. theor. Biol. (1987) **126**, 457-482

On the Relation Between Extended Forms of the Sinusoidal Perfusion and of the Convection–Dispersion Models of Hepatic Elimination†

L. BASS, M. S. ROBERTS‡ AND P. J. ROBINSON

Department of Mathematics, University of Queensland, Brisbane, Australia and ‡ School of Pharmacy, University of Tasmania, Hobart, Australia; now at the University of Otago, Dunedin, New Zealand

(*Received* 12 *May* 1986, *and in revised form* 10 *February* 1987)

Two models of hepatic elimination, the distributed sinusoidal perfusion model, and the convection-dispersion model, are extended and then compared for first order kinetics in the steady-state. The sinusoidal perfusion model is extended by the inclusion of intrahepatic sites of mixing between sinusoids. The degree of such mixing is estimated for taurocholate elimination by isolated perfused rat livers by a comparison of anatomical and kinetic estimates of uptake heterogeneity, using previously published data. The dispersion model is generalized by the inclusion of distributions of enzyme activity along the flow. Direct comparison of the two models in the limit in which the degree of dispersion is small, allows the flow-dependence of the dispersion coefficient to be determined, thereby greatly extending the explanatory power of the convection-dispersion model. Finally, the effect of intrahepatic mixing sites on uptake by Michaelis-Menten kinetics is quantified in terms of the distributed sinusoidal perfusion model, with results which may be applicable to capillary beds in general.

1. Introduction

Much recent modelling of the uptake of drugs and other substances by the intact liver has been based on the concept of transport of substrate by unidirectional convection through independent tubes or passageways (sinusoids) lined with cells containing enzymes (Brauer *et al.*, 1956; Goresky, 1963; Bass *et al.*, 1976, 1978; Forker & Luxon, 1978). Each sinusoid accepts a common input (arterial) concentration of substrate, which is depleted as it passes to the venous end of the sinusoid. In the *undistributed* sinusoidal perfusion model, these outputs are all identical, but in the more realistic *distributed* sinusoidal perfusion model, differences in sinusoidal properties bring about differences in the outputs, which must be appropriately averaged to represent the mixing of all the individual sinusoidal outputs. A limitation of these sinusoidal perfusion models is their failure to include intermixing between sinusoids (Roberts & Rowland, 1986*a*), as seen in detailed anatomical studies of the hepatic microcirculation (Koo *et al.*, 1975). Hepatic sinusoids are observed to have many interconnections with adjacent sinusoids "like the rungs of a ladder" (Koo *et al.*, 1975). Such interconnections imply a measure of mixing between

† Address correspondence to: Professor L. Bass, Department of Mathematics, University of Queensland, St. Lucia, Q. 4067, Australia.

0022-5193/87/120457+26 $03.00/0 © 1987 Academic Press Inc. (London) Ltd

sinusoids before final mixing at the liver output. Despite this limitation, the sinusoidal perfusion model, in its distributed form (in which the individual sinusoids are not functionally identical), has been successful in analyzing much of the available data on hepatic elimination, in particular the variation of hepatic uptake of substances as the steady rate of blood flow is varied (Brauer *et al.*, 1956; Pang & Rowland, 1977; Keiding & Chiarantini, 1978; Bass & Robinson, 1979; Bass, 1980; Keiding & Priisholm, 1984).

A generalized model of hepatic elimination, recently introduced by Roberts & Rowland (1985, 1986*a*), abandons the concept of non-interacting, independent sinusoids in favour of combining unidirectional convection with a diffusion-like term to account for substrate transport through the liver. The model extends the convection-diffusion transport model of Perl & Chinard (1968) by replacing the diffusion coefficient with a generalized dispersion coefficient, and by including a metabolic sink of substrate. Related convection-dispersion models have a long history in physical chemistry and chemical engineering literature, beginning with Langmuir (1908): see, for example, Wen & Fan (1975) for an overview.

A major limitation of the model of Roberts & Rowland (1985, 1986*a*) is that the physiological interpretation of the dispersion coefficient in the liver is problematical. In particular, the model does not predict how the dispersion coefficient changes with the rate of hepatic blood flow. There is thus a whole class of crucial experimental data (Brauer *et al.*, 1956; Pang & Rowland, 1977; Keiding & Chiarantini, 1978; Keiding & Priisholm, 1984) to which the convection-dispersion model, in its present form, does not relate. A further difficulty is that the dispersion model, necessarily expressed in terms of a second order partial differential equation, requires boundary conditions (additional to those of the sinusoidal perfusion model) that have not yet been formulated unambiguously. Moreover, as developed so far, the dispersion model has employed the simplifying assumption that hepatocellular enzymes are distributed uniformly along the flow. Such a simplification excludes a major theme of current hepatic pharmacokinetics: the kinetic effects of observed continuous distributions of hepatocellular enzyme activities organized in relation to the direction of hepatic blood flow (Gumucio & Miller, 1981; Bass, 1981, 1986).

In the present paper we extend the distributed form of the sinusoidal perfusion model in the steady-state to take into account intrahepatic mixing of substrate between sinusoids. By comparing anatomical estimates of sinusoidal heterogeneity with kinetic estimates of the degree of functional heterogeneity for the liver as a whole, we are able to obtain a quantitative measure of such intrahepatic mixing. Next, by considering the convection-dispersion model for small values of the dispersion coefficient, we are able to circumvent the problem of specifying the additional boundary conditions. Moreover, we incorporate distributions of hepatocellular enzyme activities along the direction of hepatic blood flow. In this limit of the dispersion model, there is a striking mathematical correspondence (Roberts & Rowland, 1986*a*) between the dispersion model and the sinusoidal perfusion model, which now allows the flow-dependence of the dispersion coefficient to be inferred, thus greatly extending the range of experimental data accounted for by the dispersion model. In particular, flow change effects which have been crucial

in discriminating between earlier models of hepatic elimination (Brauer *et al.*, 1956; Keiding & Chiarantini, 1978; Bass 1980; Keiding & Priisholm, 1984), can now be understood quantitatively in terms of the convection-dispersion model.

In the final section we depart from first-order kinetics and quantify effects of intrahepatic mixing between sinusoids on organ uptake by Michaelis-Menten kinetics, in terms of the distributed sinusoidal perfusion model. The quantification of organ heterogeneity is found to be modified in such a way that both heterogeneity and intrahepatic mixing can be estimated, or at least bounded, from data spanning the Michaelis-Menten concentration range. We illustrate these new results using previously published data on the uptake of galactose by pig livers (Keiding *et al.*, 1976).

2. Sinusoidal Perfusion Model and Intrahepatic Mixing Between Sinusoids

In the sinusoidal perfusion model, substrates are transported along the sinusoids only by unidirectional convective flow. The concentration $c(x, t)$ of substrate in the sinusoid as a function of distance x along the sinusoid and of time t is given by

$$\alpha\frac{\partial c}{\partial t}+f\frac{\partial c}{\partial x}=-\rho(x)g(c) \tag{1}$$

where α is the cross-sectional area of the sinusoid, f is the rate of blood flow through the sinusoid, $\rho(x)$ is the maximum (saturated) eliminating activity of the relevant hepatocellular enzyme at any position x, and $g(c)$ describes the dependence of the elimination rate on the local substrate concentration. Although eqn (1) has been solved for Michaelis-Menten kinetics ($g(c)=c/(c+K_m)$) both in the steady (Bass *et al.*, 1976) and unsteady (see Bass *et al.*, 1983) states, it is sufficient for our present purpose to restrict our attention to the steady-state ($\partial c/\partial t=0$), and initially, to first-order elimination kinetics ($g(c)=c/K_m$). Under these conditions, eqn (1) may be integrated over the length L of the sinusoid to give

$$\ln(c_i/c_o)=v_{\max}/(fK_m) \tag{2}$$

where c_i is the arterial (input) substrate concentration at $x=0$, c_o is the sinusoidal output concentration at $x=L$, and $v_{\max}=\int_0^L \rho(x)\,dx$ is the total maximum elimination capacity of the sinusoid. Note that eqn (2) does not depend on the functional form of $\rho(x)$. Note also that eqn (2) is equivalent to availability $c_o/c_i=\exp(-v_{\max}/fK_m)$ for a single sinusoid.

In the *distributed* sinusoidal perfusion model, a large number of such sinusoids, each with its own value of $v_{\max}/fK_m$, are arranged in parallel (in a functional rather than a geometrical sense). Each sinusoid has the common input concentration c_i; mixing of sinusoidal outputs forms the measured output concentration $\bar{c}_o$, which is the flow-weighted mean of individual sinusoidal outputs (Bass *et al.*, 1978). It has been assumed hitherto that each sinusoid acts as an independent unit, with no interaction with its neighbours until outputs are mixed in the hepatic vein or venules. Observed input and output substrate concentrations c_i and $\bar{c}_o$ are related for first

order kinetics by

$$\ln (c_i/\bar{c}_o) = \frac{V_{max}}{FK_m} - \tfrac{1}{2}\varepsilon^2\left(\frac{V_{max}}{FK_m}\right)^2 + R \tag{3}$$

where V_{max} is the total elimination capacity for the liver as a whole, and F is the rate of total hepatic blood flow. Here ε is the coefficient of variation of the (flow-weighted) maximum sinusoidal arterial-venous concentration differences v_{max}/f, and is a measure of the degree of functional heterogeneity of the liver. The Michaelis constant K_m is assumed to be the same in all sinusoids since it represents a molecular property for any one substrate-enzyme combination. For a liver made up of a number of sinusoidal groups in parallel ("notional sub-organs"), each consisting of identical sinusoids and having its own $V_{max}^{(p)}$ and $F^{(p)}$, where $\sum_p V_{max}^{(p)} = V_{max}$ and $\sum_p F^{(p)} = F$, it has been shown that ε^2 is given by (Bass, 1983)

$$\varepsilon^2 = \sum_p \frac{(V_{max}^{(p)}/V_{max})^2}{F^{(p)}/F} - 1. \tag{4}$$

The superscript "p" is chosen to designate *parallel* elements.

In equation (3), R is a positive remainder term for which there are precise upper and lower bounds, provided that ε is small enough for the quantity $v_0 = 1/\varepsilon - \varepsilon V_{max}/FK_m$ to be positive (Bass, 1980)

$$-\ln\left\{1 - \frac{e^{-v_0^2/2}}{\sqrt{2\pi}\left(\frac{v_0}{2} + \sqrt{\frac{v_0^2}{4}+1}\right)}\right\} < R \leq -\ln\left\{1 - \frac{e^{-v_0^2/2}}{\sqrt{2\pi}\left(\frac{v_0}{2} + \sqrt{\frac{v_0^2}{4}+\frac{2}{\pi}}\right)}\right\}. \tag{5}$$

It is apparent that as ε^2 decreases, R falls off much faster than ε^2. For several data sets of interest it has been shown that the remainder term R in eq (3) is small compared with the preceding term $\frac{1}{2}\varepsilon^2(V_{max}/FK_m)^2$ (Bass, 1980). This will be found again below for the data of Pries *et al.* (1981). It should be emphasised, however, that the resulting expression without R is only an approximation to the distributed sinusoidal perfusion model. For cases when R is not small, other methods of data analysis have been described (Bass *et al.*, 1983).

Note that since the term involving ε^2 in eqn (3) is negative, the effect of sinusoidal functional heterogeneity, at given values of V_{max} and F for the liver as a whole, is to increase the output substrate concentration $\bar{c}_o$ above the output concentration from an undistributed liver with the same V_{max}, K_m and F, but with functionally identical sinusoids ($\varepsilon^2 = 0$). Any unequal sharing of enzymatic elimination capacity and blood flow among the sinusoids of a liver therefore results in a reduced capacity of the liver as a whole to eliminate substrate (except in the special case in which the relevant enzyme is everywhere saturated).

We now consider the effect of mixing of substrate between parallel sinusoids at discrete sites along the flow, in order to more closely approximate the observed features of the hepatic microcirculation (Koo *et al.*, 1975). We introduce $N-1$ additional mixing sites between the input and output of the liver—see Fig. 1. These mixing sites divide the model liver into N liver "units" in series which are assumed each to behave according to the distributed sinusoidal perfusion model, with the

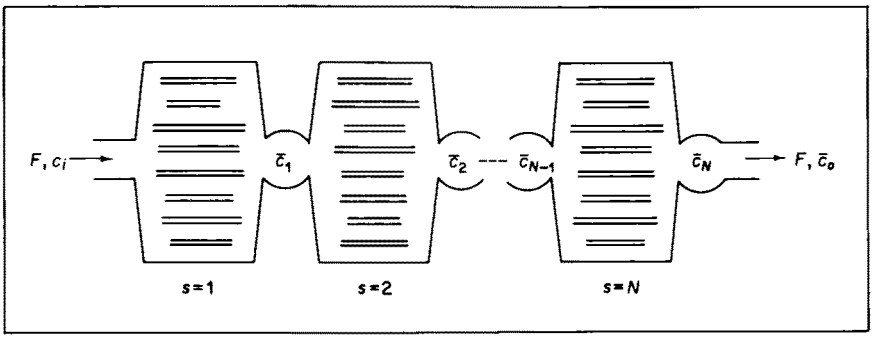

FIG. 1. Schematic representation of the sinusoidal perfusion model, with N mixing sites represented by circles. Input for each liver unit (except the first) is made up of the completely mixed outputs from sinusoids in the preceding unit. Each liver unit is described by the distributed sinusoidal perfusion model with a coefficient of variation $\varepsilon_{(s)}$. Rate F of blood flow is the same through each unit.

output from unit $s-1$ forming the input for unit s ($s = 1, 2, \ldots, N$). The index "s" is chosen to designate *serial* elements. Thus, for unit s (neglecting the remainder term R)

$$\ln(\bar{c}_{s-1}/\bar{c}_s) = \frac{V_{\max}^{(s)}}{FK_m} - \tfrac{1}{2}\varepsilon_{(s)}^2\left(\frac{V_{\max}^{(s)}}{FK_m}\right)^2 \tag{6}$$

where $V_{\max}^{(s)}$ is the total elimination capacity for the unit, and $\varepsilon_{(s)}$ is a measure of the degree of functional heterogeneity within the unit, analogous to that previously introduced for the whole liver. The relation of this simplified mixing scheme to hepatic physiology will be discussed further at the end of section 3.

For N such units in series, we have

$$\sum_{s=1}^{N} \ln(\bar{c}_{s-1}/\bar{c}_s) = \sum_{s=1}^{N}\left\{\frac{V_{\max}^{(s)}}{FK_m} - \tfrac{1}{2}\varepsilon_{(s)}^2\left(\frac{V_{\max}^{(s)}}{FK_m}\right)^2\right\}. \tag{7}$$

The output from each element is the input into the next element. In the sum on the left-hand side of eqn (7), each intermediate concentration appears in two logarithmic terms which cancel; only the terms involving the input (arterial) concentration c_i and the output (venous) concentrations $\bar{c}_o = \bar{c}_N$ survive (because they appear only once), with the result

$$\ln(c_i/\bar{c}_o) = \frac{V_{\max}}{FK_m} - \frac{1}{2}\frac{1}{(FK_m)^2}\sum_{s=1}^{N}(\varepsilon_{(s)}V_{\max}^{(s)})^2 \tag{8}$$

where we write

$$V_{\max} = \sum_{s=1}^{N} V_{\max}^{(s)} \tag{9}$$

for the total elimination capacity of the liver. Comparison of eqn (8) with eqn (3) (with $R = 0$), applicable to the liver as a whole, leads to the relation

$$\varepsilon^2 = \sum_{s=1}^{N} \varepsilon_{(s)}^2\left(\frac{V_{\max}^{(s)}}{V_{\max}}\right)^2. \tag{10}$$

Thus ε^2 is an appropriately weighted mean of the values of $\varepsilon^2_{(s)}$ of the individual units in series. This important result shows that the basic equations of the distributed sinusoidal perfusion model with first-order kinetics do not change when the assumption of the independence of sinusoids is dropped: it is the interpretation of the quantity ε^2 that is changed. This is not the case for saturation kinetics (section 6).

If we assume further that, to a first approximation, each of the N units has a similar value of $V^{(s)}_{max}$, so that $V^{(s)}_{max} \simeq V_{max}/N$; and a similar value of $\varepsilon^2_{(s)} \simeq \varepsilon^2_{loc}$ (the subscript "*loc*" signifying "local" heterogeneity) then, from eqn (10)

$$\varepsilon^2 \simeq \frac{\varepsilon^2_{loc}}{N}. \tag{11}$$

For a given degree of local heterogeneity ε^2_{loc}, therefore, the overall organ heterogeneity ε^2 is roughly inversely proportional to the number N of effective mixing sites. Local heterogeneity is in general greater than organ heterogeneity; for large values of N, ε becomes small, and the model approaches the undistributed sinusoidal perfusion model (Brauer *et al.*, 1956; Bass *et al.*, 1976). This is because a high degree of intermediate mixing tends to equalize output concentrations from individual sinusoids.

3. Estimation of the Effective Number N of Mixing Sites from Experimental Data

Estimates of sinusoidal heterogeneity on a small scale (ε^2_{loc}) may be made by investigating variations of properties of neighbouring sinusoids that may affect uptake. For example, variations in sinusoidal length, sinusoidal cross-sectional area, and sinusoidal flow velocities are all observable with a microscope in the transilluminated liver (Koo *et al.*, 1975), at least in peripheral hepatic domains. On the other hand, estimates of whole organ heterogeneity (ε^2) are obtained from the uptake properties of the intact liver by kinetic methods (see, for example Bass *et al.*, 1983). Comparison of such estimates of ε^2_{loc} and $\varepsilon^2 \simeq \varepsilon^2_{loc}/N$ allows estimates of the effective number N of idealized mixing sites in the liver to be made.

(A) ANATOMICAL ESTIMATES OF HETEROGENEITY

Koo *et al.* (1975) observed the hepatic microcirculation microscopically in the transilluminated liver of the rat, and classified hepatic sinusoids according to their topographic arrangements into three populations: direct, branching and interconnecting sinusoids. Interconnecting sinusoids were described as linking "two parallel adjacent branching sinusoids . . . like the rungs of a ladder"; here we shall take them as performing the function of intrahepatic mixing. The direct sinusoid "apparently forms a direct short transit channel from a terminal order 4 portal venule to a terminal order 4 hepatic venule, while a branching sinusoid arising from an order 4 portal venule divides into branches along a long, tortuous course before the terminal branches join several adjacent order 4 hepatic venules" (Koo *et al.*, 1975). Thus, if L_d and L_b are the lengths of direct and branching sinusoids respectively, then $L_b \gg L_d$. Koo *et al.* (1975) further observed that the diameters of these types of sinusoid did not differ significantly from each other, while their associated flow

velocities were $v_d = 0{\cdot}41 \pm 0{\cdot}039$ mm s^{-1} and $v_b = 0{\cdot}27 \pm 0{\cdot}058$ mm . s^{-1}. The relative abundances of the sinusoidal types are assumed here to be proportional to the numbers of vessels of each type actually observed, thus: $w_d = 139/515 = 0{\cdot}27$, and $w_b = 304/515 = 0{\cdot}59$. The remaining fraction 0·14 comprised the interconnecting sinusoids; for simplicity, we shall neglect their elimination capacity.

We now estimate local functional heterogeneity ε^2_{loc} based on these observations. The striking difference between the direct and branching sinusoids is their length. If we assume uniform distribution of enzyme along the sinusoids, then the total V_{max} for a sinusoid is proportional to its length, and the direct and branching sinusoids have widely differing V_{max} values. This we assume to be the principal determinant of local functional heterogeneity. Using the concept of notional sub-organs in parallel as described above, in the present context of two populations of sinusoids, eqn (4) gives an estimate of the degree of local heterogeneity

$$\varepsilon^2_{loc} \simeq w_d \frac{(V^d_{max}/V_{max})^2}{F^d/F} + w_b \frac{(V^b_{max}/V_{max})^2}{F^b/F} - 1 \tag{12}$$

where V^d_{max}, V^b_{max} and F^d, F^b are the contributions to total V_{max} and to the total rate of blood flow attributable to direct and branching sinusoids respectively. Assuming sinusoidal v_{max} to be proportional to sinusoidal length, and considering that flow rate is proportional to sinusoidal flow velocity (the sinusoidal diameters being about equal—Koo *et al.*, 1975), eqn (12) becomes

$$\varepsilon^2_{loc} \simeq w_d \frac{[L_d/(w_dL_d + w_bL_b)]^2}{v_d/(w_dv_d + w_bv_b)} + w_b \frac{[L_b/(w_dL_d + w_bL_b)]^2}{v_b/(w_dv_d + w_bv_b)} - 1. \tag{13}$$

As $L_b \gg L_d$ and w_bw_d, we have $w_bL_b \gg w_dL_d$; as $v_b < v_d$, we have also $w_bL_b^2/v_b \gg w_dL_d^2/v_d$. Using these inequalities, we neglect the first term on the right-hand side of eqn (13) because it is of the order $(L_d/L_b)^2$; the second term is $1 + (w_dv_d)/(w_bv_b)$ to the same accuracy, so that $\varepsilon^2_{loc} \simeq (w_dv_d)/(w_bv_b) = (0{\cdot}27 \times 0{\cdot}41)/(0{\cdot}59 \times 0{\cdot}27) = 0{\cdot}69$. To this approximation the direct sinusoids act essentially as a shunt of the eliminating system (Bass, 1983). It is clear how these coarse estimates could be improved with better anatomical knowledge. We note that this value of ε_{loc} is a coarse anatomical prediction of the coefficient of variation of the distribution of transit times through the liver of any intravascular indicator, if extra-sinusoidal transit times are uniformly distributed (Goresky, 1983).

(B) KINETIC ESTIMATE OF HETEROGENEITY

In contrast to the foregoing calculation of local heterogeneity based on anatomical and haemodynamic considerations, we now calculate the effective degree of functional heterogeneity of the liver as a whole, based on previously published data on the extraction of taurocholate by isolated, perfused rat livers at different steady rates of hepatic blood flow F. Pries *et al.* (1981) measured the effect on the fractional extraction of taurocholate of varying the total hepatic blood flow rate F from 0·65 to 3·55 ml . min^{-1} . g^{-1} liver in a total of 33 livers (Fig. 2). On the basis of the undistributed model for hepatic uptake, one would expect a direct proportionality

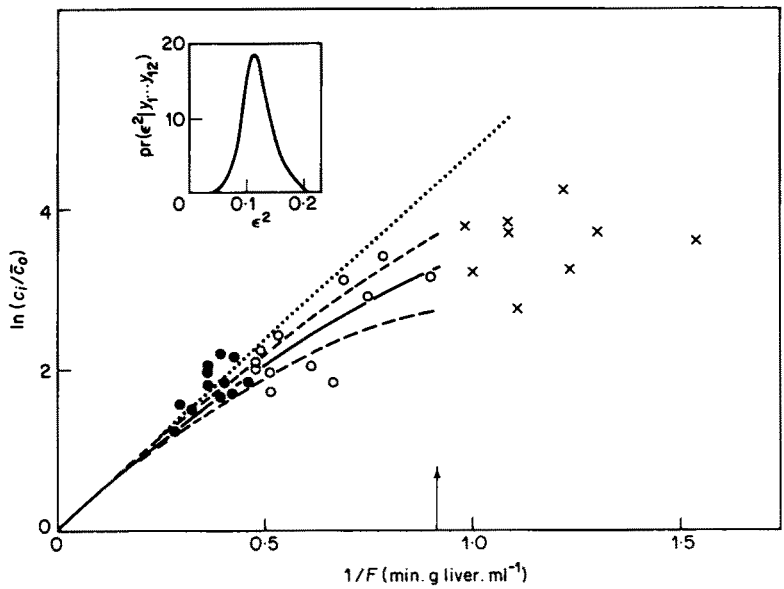

FIG. 2. Effect of perfusate flow rate F on extraction of taurocholate by isolated perfused rat livers. Experimental points are from Pries *et al.* (1981). Only the 24 data points at flow rates above 1·1 ml . min^{-1} g^{-1} liver (vertical arrow) are used in the analysis, split into two equal groups (open and closed circles) according to perfusate flow. The dotted line represents a linear regression through the origin and the solid circles, with slope $V_{max}/K_m = 4{\cdot}74$ ml . min^{-1} . g^{-1} liver. Open circles are used to construct a probability density of the parameter ε^2 (inset), with a most probable value of $\varepsilon^2 = 0{\cdot}12$. There is a 95% probability that ε^2 lies in the range (0·07, 0·17) and that the theoretical curve lies between the two broken curves.

between $\ln(c_i/\bar{c}_o)$ and $1/F$ (eqn (3) with $\varepsilon^2 = 0$ and $R = 0$), shown in Fig. 2 as the dotted straight line through the origin. With increasing $1/F$ (decreasing flow-rate), the data in Fig. 2 fall increasingly short of this straight line. That trend is predicted by the distributed model as a result of the second term on the right-hand side of eqn (3).

When quantifying ε^2 from this deviation from the undistributed model, three conditions must be satisfied. Firstly, as the hepatic blood flow is changed, there should be no change in the total number of operative sinusoids (no recruitment or de-recruitment of sinusoids). If blood flow is sufficiently reduced, sinusoids may collapse, reducing the total V_{max} of the liver and hence the slope V_{max}/K_m (Brauer *et al.*, 1956). Such sinusoidal collapse, if present and not taken into account, would lead to an overestimate of ε^2. However, the constancy of physiological control data such as O_2 consumption and galactokinase V_{max} has been demonstrated at flow values down to 1·1 ml . min^{-1} . g^{-1} liver in isolated, perfused rat livers (Keiding & Chiarantini, 1978; Keiding *et al.*, 1980). Thus no closure (de-recruitment) of sinusoids occurs at values of $1/F$ up to $(1/F)_{max} = 0{\cdot}91$ ml^{-1} . min . g liver. Then the deviations from a straight line through the origin in a plot of $\ln(c_i/\bar{c}_o)$ versus $1/F$, at $1/F$ values below $(1/F)_{max}$, refute the undistributed sinusoidal perfusion model (Pang & Rowland, 1977) and may be used to estimate organ heterogeneity (Bass, 1980).

Secondly, in order to calculate ε^2 from the first two terms of eqn (3), the magnitude of the remainder term R must be shown to be sufficiently small as compared with $\frac{1}{2}\varepsilon^2(V_{max}/FK_m)^2$. Proceeding by iteration, we first neglect R in order to determine ε^2, and then show, using bounds on R given by the inequalities (5), that indeed R is sufficiently small, compared with $\frac{1}{2}\varepsilon^2(V_{max}/FK_m)^2$, to justify its neglect in eqn (3). Since R is largest at the smallest value of F, we calculate with $(1/F)_{max}$. For the value $\varepsilon^2 = 0{\cdot}12$ estimated below, $v_0 = 1/\varepsilon - \varepsilon V_{max}/FK_m = 1{\cdot}39$. Lower and upper bounds on R, calculated from the inequalities (5), are 0·082 and 0·090 respectively. The magnitude of R is therefore less than 10% that of the preceding term in eqn (3), $\frac{1}{2}\varepsilon^2(V_{max}/FK_m)^2 = 1{\cdot}12$, thus justifying the neglect of the remainder term in this case.

Thirdly, we note that the negative term $-\frac{1}{2}\varepsilon^2(V_{max}/FK_m)^2$ on the right-hand side of eqn (3) is explicitly proportional to $(1/F)^2$. If this term is to account for the concave deviation of the solid curve in Fig. 2 from the initial straight line, ε^2 must be independent of F or vary sufficiently slowly with F, as discussed by Bass (1980). For example, if the hepatic blood flow is changed by a factor q, then the constancy of ε^2 follows from eqn (4) provided that all sinusoidal flow rates are also changed by the same factor q.

In order to exclude effects of recruitment, we estimate ε^2 and V_{max}/K_m from the 24 data points in Fig. 2 which belong to flow-rates exceeding 1·1 ml . min^{-1} . g^{-1} liver. From eqn (3) we know that at high rates of flow (low $1/F$), $\ln(c_i/\bar{c}_o)$ tends to $(V_{max}/K_m)(1/F)$, independent of ε^2. This prior theoretical knowledge suggests the use of a data-splitting procedure which reduces the two-parameter estimation problem to two separate single-parameter estimations, and which leads naturally to a Bayesian analysis of probabilities (Bass & Robinson, 1981; Robinson *et al.*, 1983).

We begin by using the 12 data points at the highest flow-rates (solid circles in Fig. 2) to calibrate V_{max}/K_m as the slope of the initial tangent of the plot, constrained to pass through the origin (since $\bar{c}_o = c_i$ when $F = \infty$). This linear regression yields the dotted straight line in Fig. 2 with the slope $V_{max}/K_m = 4{\cdot}74$ ml . min^{-1} . g^{-1} liver. The remaining 12 data points at low flow rates (open circles in Fig. 2), which are reserved for estimation of ε^2, are all located below the dotted straight line as predicted by eqn (3). The probability of this occurring by chance is 2^{-12}, a result which bears out our choice of data-splitting as well as our expectation that information about the value of ε^2 is implicit in the data. To extract this information we proceed as follows. We denote the 12 observed ordinates $\ln(c_i/\bar{c}_o)$ of the open circles in Fig. 2 by y_k, $k = 1, 2 \ldots 12$. For any postulated value of ε^2, there are 12 corresponding values of $\ln(c_i/\bar{c}_o)$ calculated from eqn (3) (with $R = 0$); these we denote by $x_k(\varepsilon^2)$, $k = 1, 2, \ldots, 12$. We then form the sum of squares of the differences

$$S^2(\varepsilon^2) = \sum_{k=1}^{m} [y_k - x_k(\varepsilon^2)]^2, \qquad m = 12. \tag{14}$$

Numerical computation shows that S^2 is an almost symmetric, U-shaped function of ε^2, with a distinctive minimum at $\varepsilon^2 = 0{\cdot}12$.

In a Bayesian approach (for example, Jeffreys, 1961; Box & Tiao, 1973), the function $[S^2(\varepsilon^2)]^{-m/2}$ transforms any prior probability density $\mathrm{pr}(\varepsilon^2)$, known before

considering the data $y_1, y_2 \ldots y_m$, into the (marginal) posterior probability density $\mathrm{pr}(\varepsilon^2|y_1, y_2, \ldots y_m)$

$$\mathrm{pr}(\varepsilon^2|y_1, y_2, \ldots, y_m) \propto \mathrm{pr}(\varepsilon^2)[S^2(\varepsilon^2)]^{-m/2} \tag{14a}$$

where $\propto$ denotes direct proportionality. (For the biological user a brief summary of the steps leading to this powerful result is given by Bass (1981) in another liver-kinetic context.) As to $\mathrm{pr}(\varepsilon^2)$, we know that $\varepsilon^2 \geq 0$ and that $\varepsilon^2 \leq \varepsilon^2_{loc} = N\varepsilon^2$ in accord with eqn (11). In the absence of other prior knowledge, it will suffice to take $\mathrm{pr}(\varepsilon^2) = \text{const.} > 0$ in the interval $0 \leq \varepsilon^2 \leq \varepsilon^2_{loc}$, and zero elsewhere. The foregoing anatomical estimate $\varepsilon^2_{loc} \simeq 0{\cdot}69$ is satisfactory in that $[S^2(\varepsilon^2)]^{-m/2}$ is practically zero for $\varepsilon^2 \geq 0{\cdot}3$, so that the precise numerical choice of ε^2_{loc} does not affect $\mathrm{pr}(\varepsilon^2|y_1, y_2, \ldots, y_m)$ calculated from eqn (14a), and shown in the inset in Fig. 2 in normalized form. This posterior probability density is approximately symmetric about a sharp peak at $\varepsilon^2 = 0{\cdot}12$, with a probability 0·95 that ε^2 lies between 0·07 and 0·17 (95% Bayesian confidence interval). Figure 2 shows the theoretical curves given by eqn (3) (with $V_{max}/K_m = 4{\cdot}74$, $R = 0$) for the most probable value $\varepsilon^2 = 0{\cdot}12$ (solid curve), for $\varepsilon^2 = 0{\cdot}07$ and $\varepsilon^2 = 0{\cdot}17$ (upper and lower broken curves). The odds are 19:1 that ε^2 takes a value such that the predicted curve lies between the two broken curves in Fig. 2. Various iterations of the foregoing procedure converge to results which make little quantitative difference to these conclusions.

We note the similarity of $\mathrm{pr}(\varepsilon^2|y_1, y_2, \ldots, y_m)$ in the inset of Fig. 2 to the corresponding probability density constructed from pig liver data, obtained from an experiment of a different design (Keiding *et al.*, 1976) by more detailed Bayesian methods (Robinson *et al.*, 1983, Fig. 2(a)), where the most probable value of ε^2 was 0·165. The foregoing data analysis illustrates again the power of data-splitting based on a prior theoretical idea (Bass & Robinson, 1981), as well as the proposition that "in the analysis of biological data involving nonlinear models, Bayesian techniques can be used with considerable success and an understanding of the assumptions made" (Robinson *et al.*, 1983).

The estimates of both local and organ heterogeneity now permit the effective number N of mixing sites in the liver to be estimated since, from eqn (11), N is approximated by the ratio $\varepsilon^2_{loc}/\varepsilon^2$. The foregoing estimate of local heterogeneity, being based on anatomical considerations (and on the assumption of proportionality of maximum enzyme elimination capacity to length of sinusoids) was obtained without reference to any particular substrate. Calculations of organ heterogeneity are based on the measured uptake of particular substrates, and thus values of ε^2 may be found to vary from case to case. Nevertheless, $\varepsilon^2 = 0{\cdot}12$ for elimination of taurocholate by rat liver hepatocytes is only slightly below the value 0·137 found for the elimination of $CrPO_4$ colloid by Kupffer cells of the RE system (Bass, 1980); both are below the upper bound of 0·182 for galactose elimination by rat liver (Bass & Robinson, 1979). Values for N calculated from eqn (11) are 5·8 for taurocholate and 5·0 for the colloid.

In comparing N for taurocholate elimination with that for elimination of colloidal $CrPO_4$, it should be remembered that two entirely different systems are involved: enzymatic elimination of taurocholate in hepatocytes, and uptake of a colloid by

the RE system of Kupffer cells. It should be noted further that the analysis of the Brauer *et al.* (1956) data has the limitation that the $CrPO_4$ colloid itself is not homogeneous, but consists of particles of different sizes that are not uniformly labelled. If the rate of RES uptake depends on colloidal size, then there is a superposition of heterogeneities of the organ and the colloid that is absent when a molecular substrate, such as taurocholate, is used.

The interpretation of N as the effective number of mixing sites that a substrate encounters while being eliminated, should not be taken as an anatomical reality in a general capillary bed: mixing is usually distributed amongst adjacent sinusoids (*via* the interconnecting sinusoids of Koo *et al.* (1975), for example), rather than taking place at N discrete hepatic mixing sites. Differences in N (or in organ heterogeneity ε^2) for different substrates and uptake systems indicate different degrees of intrahepatic mixing. This may be due to the regions of elimination of the various substrates extending over different sinusoidal lengths (Gumucio & Miller, 1981), with different substrates having different "contact times" with enzymes, so that the elimination of different substrates may take place over regions that encompass different numbers of effective mixing sites.

A simple self-consistent interpretation of the present mixing scheme is obtained by reconsidering the single-capillary models of capillary beds in general (Renkin, 1959; Crone, 1963), and of the liver in particular. Suppose that only the most closely related, nearest-neighbour pairs of sinusoids (capillaries) interact prior to venous mixing. When each serial element in Fig. 1 involves only two (non-identical) sinusoids, the mixing sites come close to anatomical reality. If the capillary bed is assumed to consist of a set of such interacting *pairs* of capillaries acting in parallel and having identical input-output relations, the single capillary (undistributed) model of the organ is replaced by a "capillary pair" model which leaves unchanged the foregoing arterial-venous relations for the whole organ (eqn (8)).

A more macroscopic, specifically hepatic interpretation of Fig. 1 leading to the same mathematical results, is to attribute N mixing sites to each acinus (Rappaport's microvascular unit: Rappaport, 1975), with a set of identical acini acting in parallel comprising the liver ("single acinus" interpretation).

The overall effect of the foregoing extension of the distributed sinusoidal perfusion model is to bring it closer to the convection-dispersion model of Roberts & Rowland (1985, 1986*a*). Despite the major differences remaining between the models, this approach will facilitate their constructive comparison in section 5.

4. Extension of the Convection–Dispersion Model

The convection-dispersion model of Roberts & Rowland (1985, 1986*a*) outlined in the "Introduction", includes a diffusion-like term which affects profoundly the mathematical description of elimination. The concentration $c(x, t)$ of substrate in the liver as a function of time t and position x along the hepatic blood flow F, satisfies the second-order partial differential equation

$$A\frac{\partial c}{\partial t}+F\frac{\partial c}{\partial x}-AD\frac{\partial^2 c}{\partial x^2}=-\rho(x)g(c) \qquad (15)$$

where A is the total cross-sectional area for flow through the liver. The metabolic sink, which extends the model of Perl & Chinard (1968), is proportional to the maximum eliminating activity $\rho(x)$ of the relevant hepatocellular enzyme at any position x, and $g(c)$ describes the dependence of the elimination rate on the local substrate concentration, as in eqn (1). The major departure from eqn (1) is the diffusion-like second derivative term $AD\,\partial^2 c/\partial x^2$, in which the dispersion coefficient D represents effects of variations of blood velocities amongst sinusoids, and of interconnections between sinusoids, on microscopic components of convection, as well as the relatively minor effects of molecular diffusion (Roberts & Rowland, 1985, 1986*a*).

In their calculations, Roberts & Rowland (1985, 1986*a*) assumed that $\rho(x)$ is constant ($\rho = V_{max}/L$), so that the relevant hepatocellular enzyme activity is spatially uniform in the liver. This restriction, which excludes effects of observed continuous distributions of enzyme activities along the direction of hepatic blood flow (see Gumucio & Miller, 1981) will be removed in what follows. Only first order kinetics, in which $g(c) = c/K_m$, was considered by Roberts & Rowland (1985, 1986*a*), and that restriction is retained in this section.

Because of the term $\partial^2 c/\partial x^2$, the solution of eqn (15) requires the imposition of additional boundary conditions at the inlet and outlet of the liver. The choice of these boundary conditions is problematical. Roberts & Rowland (1985) initially chose the well-known Dankwerts conditions (Dankwerts, 1953; Wen & Fan, 1975); however, other boundary conditions may be appropriate for the liver, as discussed by Roberts & Rowland (1986a). In general, the choice of boundary conditions affects critically the solution of eqn (15) both in the steady and unsteady states. However, in the steady-state, and for small values of the dispersion coefficient, the implications of the dispersion model become independent of the additional boundary conditions. In the present paper, for the purposes of comparing constructively the convection-dispersion model with the extended sinusoidal perfusion model, we confine ourselves to this unambiguous limiting case.

In the steady state with $g = c/K_m$, eqn (15) becomes

$$\frac{dc}{dx} - LD_N \frac{d^2c}{dx^2} = -\rho(x)\frac{c}{FK_m} \tag{16}$$

where we have retained the spatial dependence of the maximum eliminating activity $\rho(x)$ of the enzyme, and where we have replaced the dispersion coefficient D with the dimensionless dispersion number D_N

$$D_N = \frac{AD}{FL} = \frac{\tau}{\tau_D}. \tag{17}$$

Here $\tau = L/(F/A)$ is the convective transit time through the liver (of length L), and $\tau_D = L^2/D$ is the characteristic dispersion time for the liver (Perl & Chinard, 1968). It is shown in Appendix A that, for small values of D_N ($D_N \ll 1$, that is $\tau \ll \tau_D$), integration of eqn (16) gives

$$\ln(c_i/\bar{c}_o) = \frac{V_{max}}{FK_m} - \left(\frac{V_{max}}{FK_m}\right)^2 \frac{\overline{\rho^2}}{\bar{\rho}^2} D_N \tag{18}$$

where c_i and $\bar{c}_o$ are the observed arterial and venous substrate concentrations, respectively, and where $\bar{\rho}$ and $\overline{\rho^2}$ are the mean and mean square values of ρ along the effective length of the liver

$$\bar{\rho} = \frac{1}{L}\int_0^L \rho \, dx = \frac{V_{max}}{L} \tag{19}$$

and

$$\overline{\rho^2} = \frac{1}{L}\int_0^L \rho^2 \, dx. \tag{20}$$

Note that the effect of non-uniformity of the hepatocellular enzyme activity ρ is expressed by the ratio $\overline{\rho^2}/\bar{\rho}^2 \geq 1$, with equality for $\rho(x) = \text{constant}$ in the interval $0 \leq x \leq L$. Suppose, for example, that the relevant enzyme is uniformly distributed over a length $l < L$ of the liver. Thus $\rho(x) = 0$ for $0 \leq x < x_1$ and for $x_1 + l < x \leq L$, while $\rho(x) = V_{max}/l$ for $x_1 \leq x \leq x_1 + l$ (Fig. 3). For such a distribution

$$\overline{\rho^2} = \frac{1}{L}\int_{x_1}^{x_1+l}\left(\frac{V_{max}}{l}\right)^2 dx = \frac{V_{max}^2}{Ll}. \tag{21}$$

Then, using $\bar{\rho} = V_{max}/L$ from eqn (19), we have

$$\frac{\overline{\rho^2}}{\bar{\rho}^2} = \frac{L}{l} = \frac{\tau}{\tau_c} \tag{22}$$

where $\tau = L/(F/A)$ is the convective transit time for the substrate through the liver, and $\tau_c = l/(F/A) < \tau$ is the time during which the substrate is actually in contact with the enzyme of (uniform) density ρ: the contact time. It is clear that the ratio τ/τ_c may become significantly larger than unity since much of the total transit time through the liver is contributed by the delivery of substrate to and from sites of

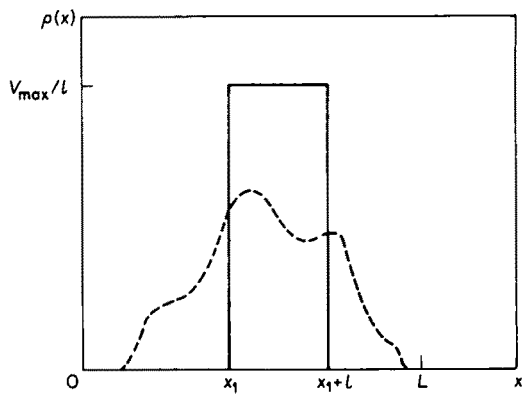

FIG. 3. Illustrative example of distribution of maximum hepatocellular enzyme activity, having density $\rho(x)$, as a function of distance along the direction of blood flow in the liver from the arterial end ($x = 0$) to the venous end ($x = L$). There is no enzyme activity between $x = 0$ and $x = x_1$, nor between $x = x_1 + l$ and $x = L$, while there is a uniform density $\rho(x) = V_{max}/l$ between $x = x_1$ and $x = x_1 + l$. The broken line represents a more physiological distribution with a smaller magnitude of $\overline{\rho^2}/\bar{\rho}^2 > 1$.

enzymatic activity, which may themselves be located in specific limited zones of the liver (see Bass *et al.*, 1983).

The difficulty of modelling hepatic D_N in terms of observable anatomic and haemodynamic features of the liver (and the absence of such modelling in the work of Roberts & Rowland, 1985, 1986*a*), suggests that D_N is to be determined from kinetic data in each particular case. We note that if this is done from kinetic relations such as eqn (18), it will be only the product $(\overline{\rho^2}/\bar{\rho}^2)D_N$ that will be determined. However, if effects of dispersion (characterized by D_N) could be separated from effects of longitudinal enzyme distributions (characterized by $\overline{\rho^2}/\bar{\rho}^2$, in particular L/l) by further analysis, then the convection-dispersion model could be brought to bear on the relation between transit times and contact times which is essential to the interpretation of bolus and other transient experiments (Goresky, 1983; Bass *et al.*, 1983).

For a more general interpretation of eqn (18) we write it as

$$\bar{c}_o/c_i = e^{-V_{max}^{eff}/FK_m}, \tag{23}$$

$$V_{max}^{eff} = V_{max}\left(1 - \frac{V_{max}}{FK_m}\frac{\overline{\rho^2}}{\bar{\rho}^2}D_N\right). \tag{24}$$

Equation (23) has the form of bioavailability $\bar{c}_0/c_i$ generated by unidirectional convective transport alone, as in the undistributed perfusion model, with V_{max} replaced by an effective value V_{max}^{eff}. However, eqn (24) shows quantitatively that V_{max}^{eff} is in general less than the organ V_{max} seen at saturation of the organ with substrate. The effective intrinsic clearance V_{max}^{eff}/K_m is smaller than the value V_{max}/K_m that would be found if transport was purely convective. This is because the concentration gradient of substrate that would be generated by the interplay of elimination with the unidirectional convective flux alone, gives rise to an additional diffusive flux (proportional to D_N) which enhances bioavailability. The transport effect of this gradient is the greater, the greater the non-uniformity of the distribution $\rho(x)$ as quantified by the ratio $\overline{\rho^2}/\bar{\rho}^2$ (in particular, the greater the ratio L/l in eqn (22)). This transport interpretation of the relation between V_{max}^{eff} and V_{max} differs from the statistical interpretation of that relation in the distributed sinusoidal perfusion model (Bass *et al.*, 1978).

5. Comparison of the Models: Flow Dependence of Dispersion

The distributed sinusoidal perfusion model has been successful in interpreting experimental data concerning the uptake of substances by the intact liver for intermediate to high bioavailabilities, especially when the steady hepatic blood flow is varied (see, for example, Brauer *et al.*, 1956; Keiding & Chiarantini, 1978; Bass & Robinson, 1979; Bass, 1980; see also section 2 above). By contrast, any analysis of the same experimental data by the convection-dispersion model would require additional hypotheses concerning the variation of the dispersion number D_N with changes in the hepatic blood flow, which have so far not been proposed.

Axial dispersion is not primarily due to axial molecular diffusion (independent of flow rate) which is a "relatively small component of overall dispersion within the liver" (Roberts & Rowland, 1985). Axial dispersion could, however, be affected by the distribution of flow velocities within each sinusoid, as demonstrated by Taylor (1953) for laminar flow through tubes. Suppose that diffusion transverse to the convective flow is relatively rapid in the sense that $L/V_o \gg d^2/3{\cdot}8^2D^o$, where L is the length of the tube, V_o is the maximum fluid velocity at the axis, d is the tube diameter and D^o is the coefficient for molecular diffusion. Then (Taylor, 1953) the axial dispersion coefficient D may be written as

$$D = \frac{d^2 V_o^2}{192 D^o}. \tag{25}$$

Since in the liver the maximum fluid velocity V_o is proportional to the rate F of hepatic blood flow, eqn (25) predicts that $D \propto F^2$, and hence, from eqn (17), $D_N \propto F$. Under these conditions, the second term on the right-hand side of eqn (18) would be proportional to $1/F$, leaving $\ln(c_i/\bar{c}_o)$ still proportional to $1/F$. This prediction would contradict several sets of experimental data on the effect of flow changes on hepatic uptake (summarised in Bass, 1980), in the same way as does the undistributed perfusion model, and in particular the data of Pries *et al.* (1981) illustrated in Fig. 2 above. However, a tube with laminar flow is far from the haemodynamic picture of the liver as envisaged by Roberts & Rowland (1985, 1986*a*). They view as the principal cause of dispersion in the liver the "branching of the sinusoids and interconnections, together with variations in the velocity and path lengths travelled by elements of blood". The variation of such a complex of processes with the rate of total hepatic blood flow appears to be difficult to model directly. However, the comparison of the dispersion model with the distributed sinusoidal perfusion model as extended in section 2 enables us to infer the flow dependence of the dispersion coefficient, which brings the convection-dispersion model into agreement with flow change data pertaining to the limiting circumstances to which the comparison will be confined.

Roberts & Rowland (1985) have already noted the formal correspondence of eqn (3) (with $R = 0$) to eqn (18) (with $\overline{\rho^2}/\bar{\rho}^2 = 1$). More physiologically, the foregoing interpretation of organ values of ε^2 in terms of intrahepatic mixing sites (eqns (10) and (11)) has brought the perfusion model closer to the convection-dispersion model, while the latter model has been extended by admitting continuous longitudinal enzyme distributions ($\overline{\rho^2}/\bar{\rho}^2 > 1$) previously included only in the sinusoidal perfusion model. Comparison of eqns (3), (11), and (18) now leads to the identification

$$(\overline{\rho^2}/\bar{\rho}^2) D_N = \tfrac{1}{2}\varepsilon^2 \simeq \tfrac{1}{2}\varepsilon_{loc}^2/N. \tag{26}$$

On this basis, the flow dependence of the dispersion coefficient can now be considered.

As distributions $\rho(x)$ of hepatocellular enzymes are fixed in liver cells, we may expect $\overline{\rho^2}/\bar{\rho}^2$ to be independent of the rate F of hepatic blood flow. We expect also the constancy of $\varepsilon^2 \simeq \varepsilon_{loc}^2/N$ under moderate changes in F (Bass, 1980), as discussed

in section 2. Equation (24) suggests therefore that D_N is approximately independent of F. From eqn (17) it follows that the *dispersion coefficient D is directly proportional to F*, in contrast to the case of laminar flow in tubes (Taylor, 1953; eqn (25) above, *et seq.*), and to the flow-independence of the molecular diffusion coefficient.

On the basis of eqn (26), experimental data from flow change experiments successfully accounted for by the distributed sinusoidal perfusion model may now be equally well described in terms of the convection-dispersion model. In particular, the experiments of Pries *et al.* (1981) on uptake of taurocholate by isolated perfused rat livers, which on the basis of the perfusion model give an estimate of $\varepsilon^2 = 0{\cdot}12$, give on the basis of the convection-dispersion model $D_N\rho^2/\bar{\rho}^2 = \frac{1}{2} \times 0{\cdot}12 = 0{\cdot}06$. For the uptake of colloidal $CrPO_4$ in the experiments of Brauer *et al.* (1956), as analyzed by Bass (1980), $D_N\rho^2/\bar{\rho}^2 = \frac{1}{2} \times 0{\cdot}137 = 0{\cdot}069$. Furthermore, the experiments of Keiding & Chiarantini (1978) on uptake of galactose by rat liver, as analyzed by Bass & Robinson (1979), gave an upper bound on ε^2 of 0·182, which translates into an upper bound on $D_N\rho^2/\bar{\rho}^2$ of 0·091.

We do not consider here the question as to how D_N might vary from substrate to substrate in a given liver preparation. Moreover, we do not analyze effects of details of data analysis, and of appropriate data selection, on all the foregoing illustrative estimates. In previous work of Roberts & Rowland (1985; 1986*a*,*b*) values of D_N (or possibly $(\rho^2/\bar{\rho}^2)D_N$), inferred for various substrates from several steady-state and transient data sets, ranged from 0·11 to 0·68. We emphasise that the correspondence between the convection-dispersion and the distributed sinusoidal perfusion models (as extended here) is restricted to the limit of small D_N and first order kinetics in the steady state. In particular, our discussion of the flow dependence of D_N is stricted accordingly. The full mathematical structures of the two models are so different that their quantitative predictions must differ greatly for general experimental situations (Bass, 1986). To provide such quantitative predictions from the models requires further theoretical analyses. In particular, a final formulation of the complete boundary conditions for the convection-dispersion model is needed. As non-linear (saturation) kinetics has provided powerful tests of the validity of models of hepatic elimination in the past (see, for example, Bass & Robinson, 1981; Bass *et al.*, 1983), the foregoing considerations need to be extended beyond first-order kinetics. In the next section we give this extension for the distributed sinusoidal perfusion model.

6. Effects of Mixing Sites on Hepatic Uptake by Michaelis–Menten Kinetics

In the case of data relating to uptake by first order kinetics at different rates of hepatic blood flow (sections 2, 3 above), the introduction of intrahepatic mixing sites into the distributed sinusoidal perfusion model led to a re-interpretation of the quantity ε^2 characterizing heterogeneity of uptake (eqn (11) above), without changing its numerical value or the manner of its determination from the data. In this section we consider effects of mixing sites on steady hepatic elimination by Michaelis-Menten (saturable) kinetics. When substrate concentrations are varied across the Michaelis-Menten range, as in the experiments of Keiding *et al.* (1976),

ε^2 now becomes itself dependent on substrate concentration, and new methods of fitting the data to the model must be devised. One such method is developed below; it is closely related to previous determinations of ε^2 in the distributed sinusoidal perfusion model (Bass *et al.*, 1978; Bass & Robinson, 1981) from the initial slope and the asymptote of an appropriate Lineweaver-Burk plot.

When first-order uptake kinetics is replaced with Michaelis-Menten kinetics (by replacing $g(c) = c/K_m$ with $g(c) = c/(c + K_m)$ in eqn (1)), the distributed sinusoidal perfusion model predicts the arterial-venous relation (Bass *et al.*, 1978, 1983):

$$\frac{c_i - \bar{c}_o}{K_m} + \ln \frac{c_i}{\bar{c}_o} = \frac{V_{\max}}{FK_m} - \tfrac{1}{2}\varepsilon^2 \left[\frac{V_{\max}}{F(K_m + \bar{c}_o)}\right]^2. \tag{27}$$

Equation (27), valid to order ε^2 of small heterogeneity, generalizes equation (3) (with $R = 0$), which is recovered when $\bar{c}_o/K_m$ and $(c_i - \bar{c}_o)/K_m$ are neglected at low substrate concentrations. In the opposite limit of large $\bar{c}_o/K_m$, the last term on the right-hand side of eqn (27) vanishes, and eqn (27) is reduced to the basic equation of the undistributed saturable sinusoidal perfusion model (Bass *et al.*, 1976). The same reduction results from setting $\varepsilon^2 = 0$ (no heterogeneity).

We now retrace the steps, associated with eqns (6) to (11), for the more general kinetics. In place of eqn (6) we have for each serial element

$$\frac{\bar{c}_{s-1} - \bar{c}_s}{K_m} + \ln \frac{\bar{c}_{s-1}}{\bar{c}_s} = \frac{V_{\max}^{(s)}}{FK_m} - \tfrac{1}{2}\varepsilon_{(s)}^2 \left[\frac{V_{\max}^{(s)}}{F(K_m + \bar{c}_s)}\right]^2 \tag{28}$$

with $s = 1, 2, \ldots, N$ and $\bar{c}_N = \bar{c}_o$: see Fig. 1. On summing over s, all intermediate concentration terms on the left-hand side cancel; using also eqn (9) we obtain

$$\frac{c_i - \bar{c}_o}{K_m} + \ln \frac{c_i}{\bar{c}_o} = \frac{V_{\max}}{FK_m} - \frac{1}{2F^2} \sum_{s=1}^{N} \varepsilon_{(s)}^2 \left(\frac{V_{\max}^{(s)}}{K_m + \bar{c}_s}\right)^2. \tag{29}$$

Comparison of eqns (27) and (29) yields

$$\varepsilon^2 = \sum_{s=1}^{N} \varepsilon_{(s)}^2 \left(\frac{V_{\max}^{(s)}}{V_{\max}}\right)^2 \left(\frac{K_m + \bar{c}_o}{K_m + \bar{c}_s}\right)^2. \tag{30}$$

Assuming again that the serial units have similar values of $\varepsilon_{(s)} = \varepsilon_{loc}$ and of $V_{\max}^{(s)} = V_{\max}/N$, we obtain the generalization of eqn (11)

$$\varepsilon^2 = \frac{\varepsilon_{loc}^2}{N} \phi \tag{31}$$

$$\phi = \frac{1}{N} \sum_{s=1}^{N} \left(\frac{K_m + \bar{c}_o}{K_m + \bar{c}_s}\right)^2. \tag{32}$$

The positive factor ϕ corrects eqn (11) for the effects of saturable kinetics. Evidently $\phi = 1$ when $N = 1$ (because $\bar{c}_N = \bar{c}_o$), and when concentrations are either very low or very high compared with K_m; and $\phi < 1$ otherwise, because $\bar{c}_o$ is the smallest of all $\bar{c}_s$ values.

Since ε^2_{loc} is determined by anatomical and haemodynamic considerations (as in section 3), it is independent of substrate concentration. In contrast, the presence of mixing sites combined with Michaelis–Menten kinetics makes the kinetically determined ε^2 dependent on substrate concentration through the factor ϕ in eqns (31) and (32). It is the factor ϕ that makes inappropriate the global fitting of a single value of ε^2 over a range of concentrations extending beyond the first-order regime, as was done for example in Robinson *et al.* (1983). We now examine quantitatively this new effect and its influence on the determination of ε^2 from steady-state data relating to saturation kinetics (Bass *et al.*, 1978; Bass & Robinson, 1981).

Equation (27) is accurate to order ε^2. When ε^2 is expressed by eqns (31) and (32), that order of accuracy is preserved by evaluating $\bar{c}_o$, $\bar{c}_s$ in eqn (32) from the undistributed model ($\varepsilon_{(s)}=0$), as this simplification leads only to errors of order ε^4. The summation in eqn (32) can then be carried out numerically for any N and any c_i by calculating the successive values of $\bar{c}_s$ from eqn (28), with $\varepsilon_{(s)}=0$. It is convenient to study the properties of ϕ, as defined by eqn (32), in terms of the normalized steady rate of elimination u

$$u = V/V_{\max} = F(c_i - \bar{c}_o)/V_{\max} \tag{33}$$

which varies on the finite interval $0 \le u < 1$. According to the saturable undistributed perfusion model (Bass *et al.*, 1976),

$$c_i/K_m = \frac{ru\, e^{r(1-u)}}{e^{r(1-u)}-1}, \qquad \bar{c}_o/K_m = \frac{ru}{e^{r(1-u)}-1}, \qquad r = V_{\max}/(FK_m). \tag{34}$$

Corresponding equations relate any $\bar{c}_{s-1}$ (in place of c_i) to $\bar{c}_s$ (in place of $\bar{c}_o$) when $V_{\max}$ is replaced by $V_{\max}/N$. We make explicit the dependence of ε^2 on u by rewriting eqn (31) as

$$\varepsilon^2(u) = \varepsilon^2(0)\phi(u), \qquad \varepsilon^2(0) = \varepsilon^2_{loc}/N \tag{35}$$

Here $\varepsilon^2(0)$ is the value of ε^2 previously calculated from first-order data ($u \to 0$). An example of the function $\phi(u)$, calculated numerically for $N=6$ and $r=3$, is shown as the solid curve in Fig. 4.

In order to gain further insight into $\phi(u)$, and to circumvent lengthy numerical calculations, we shall approximate $\phi(u)$ for the case $N \gg 1$ by replacing the sum in eqn (32) by an integral, and then use the result to obtain upper and lower bounds on the exact $\phi(u)$. This is done in Appendix B, where the integral approximation to $\phi(u)$ is shown to be a lower bound, $\phi_-(u) \le \phi(u)$, for any $N \ge 1$

$$\phi_-(u) = \frac{1}{r}\left(1 + \frac{ru}{e^{r(1-u)}-1}\right)^2 \ln \frac{1 + \dfrac{e^{r(1-u)}-1}{ru}}{1 + \dfrac{e^{r(1-u)}-1}{ru\, e^{r(1-u)}}}. \tag{36}$$

The lower broken curve in Fig. 4 is a plot of eqn (36) for $r=3$. It is also shown in Appendix B that a corresponding upper bound, $\phi_+(u) \ge \phi(u)$, for any particular value of N, is given by

$$\phi_+(u) = \phi_-(u) + \frac{1}{N}\left[1 - \left(\frac{e^{r(1-u)} + ru - 1}{(1+ru)\, e^{r(1-u)} - 1}\right)^2\right] \tag{37}$$

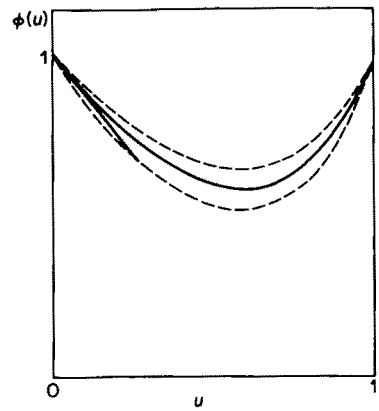

FIG. 4. The function $\phi(u)$, $u = V/V_{max}$, exemplified for $r = V_{max}/FK_m = 3$ and $N = 6$. The solid curve is from numerical calculation based on eqn (32). Upper and lower bounds on $\phi(u)$ (upper and lower broken curves) are calculated from analytical expressions given by eqns (36) and (37). The lower bound is valid for all N. The solid straight line represents the linear approximation to $\phi(u)$ used in the calculation of the asymptote of the curved Lineweaver-Burk plot. It is extended over the interval of u containing the data used in the determination of the asymptote.

where $\phi_-(u)$ is given by eqn (36). The upper bound is illustrated in the upper broken curve in Fig. 4 for $N = 6$ and $r = 3$. At high N the bounds ϕ_-, ϕ_+ become close approximations to the exact function $\phi(u)$.

If we know the factor $\phi(u)$ from these or other (especially numerical) considerations, we are able to construct the appropriate curved Lineweaver-Burk plot of the sinusoidal perfusion model in the presence of mixing sites, valid to order ε^2. Dividing eqn (27) (with the generalized ε^2 given by eqn (35)) through by $(c_i - \bar{c}_o)/K_m = ru$, and substituting for $\bar{c}_o/K_m$ from the second of eqns (34) gives

$$1 + K_m/\hat{c} = \frac{1}{u}\left[1 - \frac{1}{2}\varepsilon^2(0)\phi(u)\frac{r}{\left(1 + \dfrac{ru}{e^{r(1-u)} - 1}\right)^2}\right], \tag{38}$$

where

$$\hat{c} = \frac{c_i - \bar{c}_o}{\ln(c_i/\bar{c}_o)} \tag{39}$$

is the logarithmic average of the input and output substrate concentrations (Bass *et al.*, 1978). Equation (38) describes a Lineweaver-Burk type plot of $1/u (= V_{max}/V)$ against $K_m/\hat{c}$, used previously in the analysis of Michaelis-Menten uptake data according to both the undistributed model ($\varepsilon^2(0) = 0$; Bass *et al.*, 1976) and the distributed sinusoidal perfusion model ($\phi(u) = 1$; Bass *et al.*, 1978; Bass & Robinson, 1981), but here generalized to take into account the effects of intrahepatic mixing ($\phi(u) < 1$). At high substrate concentrations ($V/V_{max} = u \to 1$) the denominator of the last terms in eqn (38) tends to infinity, reducing that equation to

$$1 + K_m/\hat{c} = 1/u. \tag{40}$$

This is the initial tangent (at the point $K_m/\hat{c}=0, 1/u=1$) of all the plots, as well as the entire plot for the undistributed perfusion model which is characterized by $\varepsilon^2(0)=0$.

We show in Appendix C that the plot of $1/u$ against $K_m/\hat{c}$, given by eqn (38) for the case of N mixing sites ($N-1$ intrahepatic mixing sites), has the asymptote at large $1/u$, $K_m/\hat{c}$

$$1+K_m/\hat{c}=\frac{1}{u}(1-\tfrac{1}{2}\varepsilon^2(0)r)+\frac{\varepsilon^2(0)r/N}{e^{r/N}-1}. \tag{41}$$

For $N=1$ we recover the asymptote pertaining to the distributed perfusion model (Bass *et al.*, 1978). The slope of the asymptote in equation (41) is, to order $\varepsilon^2(0)$

$$\mathrm{d}(1/u)/\mathrm{d}(K_m/\hat{c})=1+\tfrac{1}{2}\varepsilon^2(0)r \tag{42}$$

whereas the corresponding slope of the initial tangent is unity (from eqn (40), or by setting $\varepsilon^2(0)=0$). The slope of the asymptote therefore exceeds that of the initial tangent by $\frac{1}{2}\varepsilon^2(0)r$, independent of intrahepatic mixing, and $\varepsilon^2(0)$ can be determined from that slope difference in the same way as in earlier work with $N=1$ (Bass *et al.*, 1978; Bass & Robinson, 1981). This is because the slope of the asymptote is determined by first-order uptake at low substrate concentrations. However, the position of the intersection between the asymptote and the initial tangent, $[(K_m/\hat{c})_{int}, (1/u)_{int}]$, does depend on N: from eqns (40) and (41) we find

$$(K_m/\hat{c})_{\mathrm{int}}=\frac{2r/N}{e^{r/N}-1}-1, \qquad (1/u)_{\mathrm{int}}=\frac{2r/N}{e^{r/N}-1}. \tag{43}$$

Here the effect of introducing intrahepatic mixing sites is the same as reducing $r=V_{\max}/FK_m$ to r/N in the distributed perfusion model. As N is increased from 1 to ∞, $(K_m/\hat{c})_{int}$ increases through the interval

$$\frac{2r}{e^r-1}-1\leq(K_m/\hat{c})_{\mathrm{int}}\leq 1 \tag{44}$$

and $(1/u)_{int}$ increases through the interval

$$\frac{2r}{e^r-1}\leq(1/u)_{\mathrm{int}}\leq 2. \tag{45}$$

We consider first the ideal case of having enough data pairs $(K_m/\hat{c}, 1/u)$ of sufficient accuracy to determine the initial tangent (which determines $r=V_{\max}/FK_m$ when F is known) and asymptote independently of each other. The slope of the asymptote yields the value $\varepsilon^2(0)$ from eqn (42). The intersection of the asymptote with the initial tangent yields the value N (to the nearest integer) from either of eqns (43). If the dependence of first-order uptake on the flow-rate F had been investigated on the same preparation, as in section 3(B), an independent check on the value of $\varepsilon^2(0)$ would be available.

Only weaker conclusions can be drawn from data available at present. We illustrate the situation for the data of Keiding *et al.* (1976) as analyzed previously by Bass & Robinson (1981) and presented in part in Fig. 5. Appropriate pooling of data on

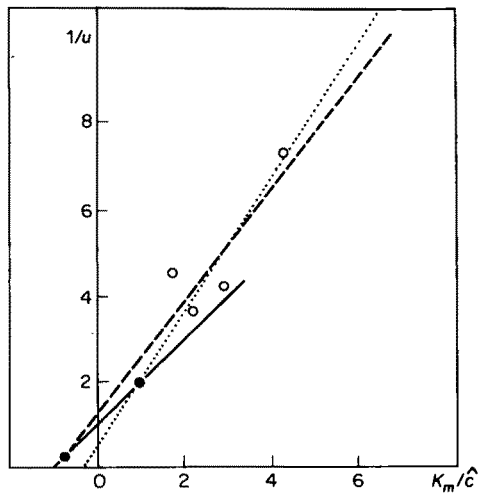

FIG. 5. Plot of $1/u = V_{max}/V$ against $K_m/\hat{c}$ for galactose elimination by isolated perfused pig livers (Keiding *et al.*, 1976). The solid straight line is the initial tangent of the plot determined from high concentration data. Broken and dotted straight lines are limiting asymptotes determined by low concentration data (open circles) and by calculated fixed points (solid circles) pertaining to the limiting cases $N = 1$ and $N = \infty$, respectively.

the elimination of galactose by six isolated perfused pig livers yielded 27 data points $(K_m/\hat{c}, 1/u)$. High concentration points determined reliably the initial tangent (and hence $r = 3{\cdot}2$), but only the four points shown in Fig. 5 were available for the determination of the asymptote. Considering the experimental errors analyzed in detail by Keiding *et al.* (1976), the determination of an asymptote from these four points alone would be grossly uncertain. Bass & Robinson (1981) were thus forced to take the intersection of the initial tangent and the asymptote, calculated from eqns (43) with $N = 1$, as a known fixed point of the asymptote (a data point of infinite weight). The resulting slope of the asymptote as fitted (shown as broken line in Fig. 5), yielded $\varepsilon^2(0) = 0{\cdot}196$ from eqn (42).

The introduction of intrahepatic mixing sites affects this procedure by allowing the fixed point of the regression to be located within the domain given by relations (44), (45). As N is increased from unity, the fixed point moves so as to make the fitted asymptote steeper. The steepest possible asymptote (dotted line in Fig. 5), associated with the limiting fixed point (1, 2) at large N, yields $\varepsilon^2(0) = 0{\cdot}351$ from eqn (42). We can thus conclude that, no matter what the value of $N \geq 1$, the data of Keiding *et al.* (1976) place $\varepsilon^2(0)$ in the range between 0·196 and 0·351. If, for example, the value $N \simeq 6$, obtained for rat liver in section 3(B) is combined with the above value of $r = 3{\cdot}2$, then $r/N = 0{\cdot}53$ gives the fixed point (0·52, 1·52) which yields a value of $\varepsilon^2(0) = 0{\cdot}30$. An interesting feature of these weak conclusions from existing data is the absolute limitation on the effect of intraphepatic mixing sites upon the magnitude of $\varepsilon^2(0)$ deduced by this analysis.

If an anatomical and haemodynamic estimate of ε^2_{loc} was made on the relevant preparation, as in section 3(A), then a value of the product $N\varepsilon^2(0) = \varepsilon^2_{loc}$ would be

available from the second of eqns (35). This would provide a check on the values of N and $\varepsilon^2(0)$ obtained kinetically if sufficiently numerous and accurate data were available. If, however, the data permit a determination of the asymptote only with the use of a calculated fixed point, knowledge of $N\varepsilon^2(0)$ permits the following iterative procedure. The limiting fixed points, pertaining to $N = 1$ and $N = \infty$, yield two limiting asymptotes as in Fig. 5, and hence some lower and upper bounds $\varepsilon_l^2(0) < \varepsilon^2(0) < \varepsilon_u^2(0)$. Then $\varepsilon_{loc}^2/\varepsilon_u^2(0) < N < \varepsilon_{loc}^2/\varepsilon_l^2(0)$ gives bounds on N which are closer together than $N = 1$ and $N = \infty$. From eqns (43), new limiting fixed points are obtained and new limiting asymptotes are drawn. This process can be repeated until a final asymptote, and hence final values of $\varepsilon^2(0)$ and N are obtained. As an example, suppose that the unknown value of ε_{loc}^2 in the pig livers of Keiding *et al.* (1976) was 0·69, as in the rat liver in section 3. Using the four low concentration data points, given in Fig. 5, to construct asymptotes throughout the iteration, we arrive at the final values $\varepsilon^2(0) = 0{\cdot}25$ and $N = 2{\cdot}8$.

The foregoing discussion shows how fundamentally the inferences from the model could be sharpened if more numerous and accurate data became available. The quantification of mixing interactions between parallel vascular pathways prior to venous mixing is likely to be of interest for capillary beds other than the liver. In this more general context, the present work continues previous progress towards increasingly physiological modelling of uptake of substances by capillary beds, initiated by the transition from formal compartments to organ models using single representative capillary structures (Renkin, 1959; Crone, 1963; Goresky, 1963; Bassingthwaighte *et al.*, 1970). The next step, to ensembles of non-interacting parallel vascular pathways with statistical distributions of uptake properties (Bass *et al.*, 1978; Forker & Luxon, 1978), is now followed by including mixing interactions in the distributed sinusoidal perfusion model on the one hand, and, on the other hand, by the convection-dispersion model of uptake (Roberts & Rowland, 1985, 1986*a*) in which the mixing interactions between parallel vascular pathways are so strong as to be described by a dispersion term in a single differential equation for the whole organ.

In order to proceed further with comparisons between the distributed perfusion model with mixing sites, and the convection-dispersion model, the latter needs to be extended quantitatively to Michaelis-Menten uptake to match the predictions of the present section. It is one of the purposes of the present paper to lay the conceptual groundwork for these forthcoming theoretical and experimental comparisons.

We are grateful to a referee for very helpful criticisms; to the Australian Research Grants Scheme and the National Health and Medical Research Council for financial support, and for the award of a National Research Fellowship to one of us (P.J.R.).

REFERENCES

BASS, L. (1980). *J. theor. Biol.* **86**, 365.
BASS, L. (1981). *J. theor. Biol.* **89**, 303.
BASS, L. (1983). *Am. J. Physiol.* **244**, G583.

BASS, L. (1986). *J. Pharm. Sci.* **75**, 321.
BASS, L., BRACKEN, A. J. & BURDEN, C. J. (1983). *Tracer Kinetics and Physiological Modelling. Lecture Notes in Biomathematics, Vol. 48* (Lambrecht, R. M. & Rescigno, A., eds). pp. 120–201. Berlin: Springer-Verlag.
BASS, L., KEIDING, S., WINKLER, K. & TYGSTRUP, N. (1976). *J. theor. Biol.* **61**, 393.
BASS, L. & ROBINSON, P. J. (1979). *J. theor. Biol.* **81**, 761.
BASS, L. & ROBINSON, P. J. (1981). *Microvasc. Res.* **22**, 43.
BASS, L., ROBINSON, P. J. & BRACKEN, A. J. (1978). *J. theor. Biol.* **72**, 161.
BASSINGTHWAIGHTE, J. B., KNOPP, T. J. & HAZELRIG, J. B. (1970). *Capillary Permeability.* (crone, C. & Lassen, N. A., eds). pp. 60–80. Copenhagen: Munksgaard.
BOX, G. E. P. & TIAO, G. C. (1973). *Bayesian Inference in Statistical Analysis.* Ch. 1, New York: Addison-Wesley.
BRAUER, R. W., LEONG, G. F., MCELROY, R. F. & HOLLOWAY, R. J. (1956). *Am. J. Physiol.* **184**, 593.
CRONE, C. (1963). *Acta Physiol. Scand.* **63**, 213.
DANKWERTS, P. A. (1953). *Chem. Eng. Sci.* **2**, 1.
FORKER, E. L. & LUXON, B. (1978). *Am. J. Physiol.* **235**, E648.
GORESKY, C. A. (1963). *Am. J. Physiol.* **204**, 626.
GORESKY, C. A. (1983). *Am. J. Physiol.* **245**, G1.
GUMUCIO, J. J. & MILLER, D. L. (1981). *Gastroenterology* **80**, 393.
JEFFREYS, H. (1961). *Theory of Probability*, 3rd edn. Oxford: Clarendon Press.
KEIDING, S. & CHIARANTINI, E. (1978). *J. Pharmacol. Exp. Ther.* **205**, 465.
KEIDING, S., JOHANSEN, S., WINKLER, K., TONNESEN, K. & TYGSTRUP, N. (1976). *Am. J. Physiol.* **230**, 1302.
KEIDING, S. & PRIISHOLM, K. (1984). *Biochem. Pharmacol.* **33**, 3209.
KEIDING, S., VILSTRUP, H. & HANSEN, L. (1980). *Scand. J. Clin. Lab. Invest.* **40**, 355.
KOO, A., LIANG, I. Y. S. & CHENG, K. K. (1975). *Q. J. Exp. Physiol.* **60**, 261.
LANGMUIR, I. (1908). *J. Am. Chem. Soc.* **30**, 1742.
PANG, K. S. & ROWLAND, M. (1977). *J. Pharmacokinet. Biopharm.* **5**, 655.
PERL, W. & CHINARD, F. P. (1968). *Circ. Res.* **22**, 273.
PRIES, J. M., STAPLES, A. B. & HANSON, R. F. (1981). *J. Lab. Clin. Med.* **97**, 412.
RAPPAPORT, A. M. (1975). *Diseases of the Liver.* (Schiff, L., ed.). pp. 1–50. Philadelphia: Lippincott.
RENKIN, E. M. (1959). *Am. J. Physiol.* **197**, 1205.
ROBERTS, M. S. & ROWLAND, M. (1985). *J. Pharm. Sci.* **74**, 585.
ROBERTS, M. S. & ROWLAND, M. (1986*a*). *J. Pharmacokinet. Biopharm.* **14**, 227, 261, 289.
ROBERTS, M. S. & ROWLAND, M. (1986b). *J. Pharm. Pharmacol.* **38**, 177.
ROBINSON, P. J., PETTITT, A. N., ZORNIG, J. & BASS, L. (1983). *Biometrics* **39**, 61.
TAYLOR, G. I. (1953). *Proc. Roy. Soc. Lond. A* **219**, 186.
WEN, C. Y. & FAN, L. T. (1975). *Models for Flow Systems and Chemical Reactors.* New York: Marcel Dekker.

APPENDIX A

An Arterial–Venous Relation for the Convection–Dispersion Model

We start from eqn (16) in the form

$$c' + \frac{\rho(x)}{FK_m} c = LD_N c'' \tag{A1}$$

where primes denote derivatives with respect to position. We assume $D_N \ll 1$ and work only to first order in D_N. Then c'' may be estimated from eqn (A1) with $D_N = 0$, since any corrections to c'' of order D_N would contribute only to order D_N^2 in the right-hand side of eqn (A1). We thus obtain

$$c'' \simeq -\frac{\rho'}{FK_m} c - \frac{\rho}{FK_m} c' \simeq \left(-\frac{\rho'}{FK_m} + \frac{\rho^2}{F^2 K_m^2} \right) c. \tag{A2}$$

Substituting for c'' from eqn (A2) in eqn (A1), dividing through with c and integrating from inlet to outlet we obtain, to order D_N

$$\ln \frac{c_i}{c_o} = \int_0^L \left(\frac{\rho}{FK_m} + LD_N \frac{\rho^2}{F^2 K_m^2} - LD_N \frac{\rho'}{FK_m} \right) \mathrm{d}x. \tag{A3}$$

The integral of the last term vanishes by taking $\rho(0) = \rho(L)$, possibly both zero for continuous distributions. Using the definitions of $\bar{\rho} = V_{\max}/L$ and of $\overline{\rho^2}$ in eqns (19) and (20), we obtain readily

$$\ln \frac{c_i}{c_o} = \frac{V_{\max}}{FK_m} - \left(\frac{V_{\max}}{FK_m} \right)^2 \frac{\overline{\rho^2}}{\bar{\rho}^2} D_N. \tag{A4}$$

Identifying c_o with the observed venous concentration $\bar{c}_o$ used in the sinusoidal perfusion model, we arrive at eqn (18).

APPENDIX B

Upper and Lower Bounds on Effects of Intrahepatic Mixing

We return to the differential equation underlying the saturable undistributed perfusion model (Bass *et al.*, 1976)

$$\frac{\mathrm{d}c}{\mathrm{d}x} = -\frac{\rho(x)}{F} \frac{c}{c + K_m} \tag{B1}$$

with any $\rho(x) \geq 0$ satisfying eqn (19). Introducing the new independent variable

$$\xi = \int_0^x \frac{L\rho(x)}{V_{\max}} \mathrm{d}x, \qquad \xi(0) = 0, \qquad \xi(L) = L, \tag{B2}$$

eqn (B1) becomes

$$\frac{\mathrm{d}c}{\mathrm{d}\xi} = -\frac{V_{\max}}{FL} \frac{c}{c + K_m} \tag{B3}$$

having the same form as eqn (B1) with a constant density $\rho = V_{\max}/L$. Hence equal division of $V_{\max}$ amongst the serial elements ($V_{\max}^{(s)} = V_{\max}/N$), used in section 6 in the transition from eqn (30) to eqns (31) and (32), corresponds to equal increments of ξ on the interval $0 \leq \xi \leq L$, no matter what the form of $\rho(x)$. Hence $\bar{c}_s = c(\xi_s)$, $\xi_s - \xi_{s-1} = L/N$.

Taking a large number of terms ($N \gg 1$) in the sum in eqn (32) with a uniform density N/L of terms on $0 < \xi \leq L$, we approximate ϕ by an integral denoted by ϕ_- in anticipation of it being a lower bound on ϕ

$$\phi_- = \frac{1}{N} \int_0^L \left(\frac{K_m + \bar{c}_o}{K_m + c(\xi)} \right)^2 \frac{N}{L} \mathrm{d}\xi = \frac{1}{L} \int_{c_i}^{\bar{c}_o} \left(\frac{K_m + \bar{c}_o}{K_m + c} \right)^2 \left(\frac{\mathrm{d}\xi}{\mathrm{d}c} \right) \mathrm{d}c. \tag{B4}$$

Substituting for $d\xi/dc$ from eqn (B3) and integrating (by partial fractions) we obtain readily

$$\phi_- = \frac{FK_m}{V_{max}}(1+\bar{c}_o/K_m)^2 \ln\frac{1+K_m/\bar{c}_o}{1+K_m/c_i}. \tag{B5}$$

Finally, from eqns (B5) and (34), we obtain eqn (36) in terms of the variable u.

We show next that $\phi_- \leq \phi(u)$ is a lower bound on $\phi(u)$, independent of N. We construct ϕ_- from $\phi(u)$ by the following process. With the mid-point of each interval (ξ_{s-1}, ξ_s) we associate an additional term in the series in eqn (32). As $dc/d\xi \leq 0$, this additional term is less than (or equal to) the term associated with ξ_s. The arithmetic mean of the resulting $2N$ terms is therefore less than ϕ. Repeating this doubling of terms, which is always associated with a reduction in their mean, we can approach ϕ_- as closely as desired. Hence $\phi_- \leq \phi$.

This result was obtained because the series in eqn (32) contains the term associated with $\xi = L$, but not the term associated with $\xi = 0$ (c_i is not amongst the $\bar{c}_s$). We obtain an *upper* bound on ϕ by considering the related series $N\phi^*$ in which the term associated with $\xi = L$ is excluded, and the term associated with $\xi = 0$ is included

$$N\phi^* = N\phi - 1 + \left(\frac{K_m+\bar{c}_o}{K_m+c_i}\right)^2. \tag{B6}$$

The analogous process of approaching ϕ_- by doubling terms now leads to the result $\phi_- \geq \phi^*$, since each term added at the mid-point of the interval (ξ_{s-1}, ξ_s) is greater than the term at ξ_{s-1}. As $N\phi^* \leq N\phi_-$, eqn (B6) yields the upper bound on ϕ

$$\phi \leq \phi_- + \frac{1}{N}\left[1-\left(\frac{K_m+\bar{c}_0}{K_m+c_i}\right)^2\right] = \phi_+. \tag{B7}$$

Using eqns (34) to express $\bar{c}_o$ and c_i in terms of u, we obtain eqn (37) for the upper bound $\phi_+(u)$.

APPENDIX C

Effect of Intrahepatic Mixing on the Asymptote of the Lineweaver–Burk Plot

To obtain eqn (41) of the asymptote from eqn (38) at large values of $K_m/\hat{c}$ and $1/u$, we need to expand the square bracket in eqn (38) in powers of the small quantity u up to order u (terms of order u^2 and higher contribute terms of only order u and higher on the right-hand side of eqn (38)). As $\phi(0) = 1$, we write

$$\phi(u) = 1 + \phi'(0)u \tag{C1}$$

where prime denotes differentiation with respect to u. Expanding the factor of $\phi(u)$ also to first order in u and collecting first-order terms of the product, we obtain from eqn (38)

$$1 + K_m/\hat{c} = \frac{1}{u}(1-\tfrac{1}{2}\varepsilon^2(0)r) + \tfrac{1}{2}\varepsilon^2(0)r\left(\frac{2r}{e^r-1} - \phi'(0)\right). \tag{C2}$$

Next we evaluate the slope $\phi'(0)$ of $\phi(u)$ at $u=0$ in the limit of first-order kinetics ($u \to 0$) by returning to eqn (32), in which sufficient accuracy is attained by using the undistributed model (as discussed in section 6): $\bar{c}_{s-1} = \bar{c}_s \exp(r/N)$, so that

$$\bar{c}_s = \bar{c}_N (e^{r/N})^{N-s}, \qquad \bar{c}_N = \bar{c}_o. \tag{C3}$$

Equation (32) thus becomes

$$\phi = \frac{1}{N} \sum_{s=1}^{N} \left(\frac{K_m + \bar{c}_o}{K_m + \bar{c}_0 e^{r(1-s/N)}} \right)^2. \tag{C4}$$

As $\bar{c}_o = 0$ corresponds to $u = 0$ according to eqn (34), we evaluate $\phi'(0)$ as

$$\left(\frac{d\phi}{du} \right)_{u=0} = \left(\frac{d\phi}{d\bar{c}_o} \right)_{\bar{c}_o=0} \left(\frac{d\bar{c}_o}{du} \right)_{u=0}. \tag{C5}$$

From eqn (34) we obtain

$$\left(\frac{d\bar{c}_o}{du} \right)_{u=0} = \frac{K_m r}{e^r - 1}. \tag{C6}$$

From eqn (C4) we obtain by differentiation at $\bar{c}_o = 0$

$$\left(\frac{d\phi}{d\bar{c}_o} \right)_{\bar{c}_o=0} = \frac{2}{NK_m} \sum_{s=1}^{N} [1 - (e^{r/N})^{N-s}]. \tag{C7}$$

From eqns (C5)-(C7) we have

$$\phi'(0) = \frac{2r}{N(e^r - 1)} \{N - [1 + e^{r/N} + (e^{r/N})^2 + \ldots + (e^{r/N})^{N-1}]\}. \tag{C8}$$

Summing the geometric series, we obtain

$$\phi'(0) = \frac{2r}{e^r - 1} \left(1 - \frac{e^r - 1}{N(e^{r/N} - 1)} \right). \tag{C9}$$

Substituting this expression for $\phi'(0)$ in eqn (C2), we obtain the desired eqn (41) of the asymptote.